Effects of rotation on the nonlinear friction of a damped dimer sliding on a periodic substrate

I. G. Neide,[1,2,*] V. M. Kenkre,[1,†] and S. Gonçalves[2,‡]

[1]*Consortium of the Americas for Interdisciplinary Science and Department of Physics and Astronomy, University of New Mexico, Albuquerque, New Mexico 87131, USA*

[2]*Instituto de Física, Universidade Federal do Rio Grande do Sul, Caixa Postal 15051, 90501-970 Porto Alegre, RS, Brazil*

(Received 12 May 2010; published 5 October 2010)

Rotational effects on the nonlinear sliding friction of a damped dimer moving over a substrate are studied within a largely one-dimensional model. The model consists of two masses connected rigidly, internally damped, and sliding over a sinusoidal (substrate) potential while being free to rotate in the plane containing the masses and the direction of sliding. Numerical simulations of the dynamics performed by throwing the dimer with an initial center of mass velocity along the substrate direction show a richness of phenomena including the appearance of three separate regimes of motion. The orientation of the dimer performs tiny oscillations around values that are essentially constant in each regime. The constant orientations form an intricate pattern determined by the ratio of the dimer length to the substrate wavelength as well as by the initial orientations chosen. Corresponding evolution of the center of mass velocity consists, respectively, of regular oscillations in the first and the third regimes, but a power law decay in the second regime; the center of mass motion is effectively damped in this regime because of the coupling to the rotation. Depending on the initial orientation of the dimer, there is considerable variation in the overall behavior. For small initial angles to the vertical, an interesting formal connection can be established to earlier results known in the literature for a vibrating, rather than rotating, dimer. But for large angles, on which we focus in the present paper, quite different evolution occurs. Some of the numerical observations are explained successfully on the basis of approximate analytical arguments but others pose puzzling problems.

DOI: 10.1103/PhysRevE.82.046601 PACS number(s): 46.90.+s, 68.35.Af, 05.60.Cd, 05.45.−a

I. MODEL AND ITS EQUATION OF MOTION

This paper is a report of some striking features we have discovered in a nonlinear model of microscopic friction. The subject of microscopic friction derives its importance from its relevance to practical technological aspects as well as the fact that there is a persistent lack of understanding in some of its aspects. Although there was a period of inactivity for centuries after the friction laws were first discovered by Leonardo da Vinci [1] and later stated by Amonton [2] and Coulomb [3], much progress has been made in the field, in the last thirty years [4–6]. Besides the connection with the microscopic origin of friction, the nonlinear dynamics that emerges from the simple system presented in this contribution is very rich and worthwhile to study. On the other hand, friction and diffusion are intrinsically related as the Einstein formula between the diffusion constant and the friction coefficient states. Indeed, the same or very similar models are frequently used to study such phenomena focusing in either of the two problems. Particularly, the diffusion of molecules in potentials [7] is an interesting problem in which rotation could have an important role. While the richness and peculiarities we observe in the nonlinear dynamics of the simple system we analyze are restricted to itself, we hope that our findings will make some contribution toward the understanding of friction and diffusion.

The physical system that stimulated our present work consists of molecules that perform internal motion such as rotation and/or vibration during the course of their meanderings over a material surface such as that of a crystal. The model we study is highly simplified, our purpose here being to understand the basic effects of nonlinearity in its dynamics as we have mentioned above, rather than to shed light on experimental features observed in microscopic friction. The model consists of a rigid rotating dimer (a pair of masses m) of length a inclined at an angle θ to the vertical as shown in Fig. 1, with its center of mass at location x moving along the horizontal, subject to a one-dimensional sinusoidal potential of half amplitude u_0 and wavelength b. The masses compris-

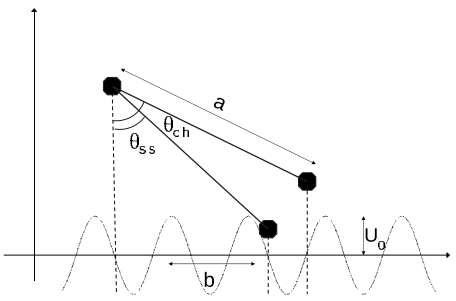

FIG. 1. Schematic depiction of the system under study. The motion of the center of mass of the dimer is along the horizontal. The two masses experience different substrate forces as a result of the difference in their locations with respect to the potential. The length of the dimer is a. The substrate potential has wavelength b and half amplitude u_0. The dimer is shown inclined to the vertical at two different angles, θ_{ch} and θ_{ss}, whose importance will be discussed in the sequel. That the two dimer positions share the same left upper mass location has no significance except drawing convenience.

*italogneide@gmail.com
†kenkre@unm.edu
‡sgonc@if.ufrgs.br

ing the dimer feel, in addition to constraining forces that maintain rigidly their separation a, the respective forces $(2\pi/b)u_0 \sin[(2\pi/b)(x \pm (a/2)\sin\theta)]$. The rotational motion occurs in the plane of the Figure (see Fig. 1) and is damped but the linear motion of the center of mass, which occurs along the horizontal, is not. Nevertheless, given that the two masses feel different substrate forces because their projections on the horizontal line (along the substrate potential) experience different phases of the potential, a coupling exists between the rotation and the center of mass motion. As a consequence, the center of mass motion is *effectively* damped.

The focus of our study is on the effects of this coupling between the rotation and the center of mass motion, specifically on the time evolution of the center of mass velocity $v(t)$ thrown initially with velocity v_0 along the substrate, along with the evolution also of the angle of rotation $\theta(t)$ and the angular velocity $d\theta(t)/dt$. We will see that fascinating results emerge, including three different regimes of motion, and that it is possible to arrive at a partial but satisfactory analytic understanding of the results.

The Lagrangian of this undamped system is clearly

$$m\left(\frac{dx}{dt}\right)^2 + \frac{ma^2}{4}\left(\frac{d\theta}{dt}\right)^2 - 2u_0 \cos\left(\frac{2\pi x}{b}\right)\cos\left(\frac{\pi a \sin\theta}{b}\right).$$

In order to facilitate the analysis, we will measure the center of mass location in units of the substrate potential wavelength, $y=2\pi x/b$, and time in units of the characteristic substrate potential period, $\tau=t(2\pi/b)\sqrt{u_0/m}$. Subsequent time differentiations, denoted by dots placed over the dimensionless y and θ, will be with respect to this τ. We will also introduce the important parameter

$$\zeta = \pi\left(\frac{a}{b}\right), \tag{1}$$

which is the full length of the dimer measured in terms of the substrate wavelength. The equations of motion for the center of mass translational motion and the dimer rotation are then, respectively,

$$\ddot{y} = (\sin y)\cos(\zeta \sin\theta),$$

$$\ddot{\theta} = (1/\zeta)(\cos y)(\cos\theta)\sin(\zeta \sin\theta) - \gamma\dot{\theta}, \tag{2}$$

where damping has been appended to the Euler-Lagrange equations via the last term in the second (angle) equation: dissipation in our system is taken to occur only in the rotation through factors not described explicitly in our model and to occur at a rate $-\gamma\dot{\theta}$.

II. NUMERICAL RESULTS

Equations (2) show explicitly that the dimer rotation and the center of mass translation are coupled to each other, and that, although there is no dissipation term in the equations proportional to its translational velocity, the center of mass motion is damped effectively because of that coupling. We have not found it possible to find exact analytic solutions of these equations. We therefore apply standard numerical techniques to determine the evolution. We find that three regimes of time evolution emerge generally as shown in Fig. 2. The transition from the first regime to the second is relatively gradual but that from the second to the third regime is quite abrupt. Initially, we incline the dimer at a nonzero angle to the vertical, $\theta_i=1.54$, give it zero initial angular velocity, and throw it along the horizontal with an initial velocity $v_0=8\pi$. Obviously, no coupling of rotation and translation occurs under these conditions if the initial angle to the vertical is either 0 or $\pi/2$. If it is different from these extremes, the center of mass velocity generally oscillates rapidly around a value higher than the initial value, showing a very small decrease in amplitude which is hardly discernible. The time for which this regime lasts exhibits a rather involved structure with divergences for certain initial angles as will be seen below. However, superimposed on that structure is a general simple tendency to increase as the initial inclination to the vertical increases. In the case shown in Fig. 1, the assumed initial inclination is close to $\pi/2$. Consequently, the time span of the first regime is very long: about 2.43×10^4 in units of the dimensionless τ. We have displayed this very long time span in two split sections in the plot, the first lasting 3000 time

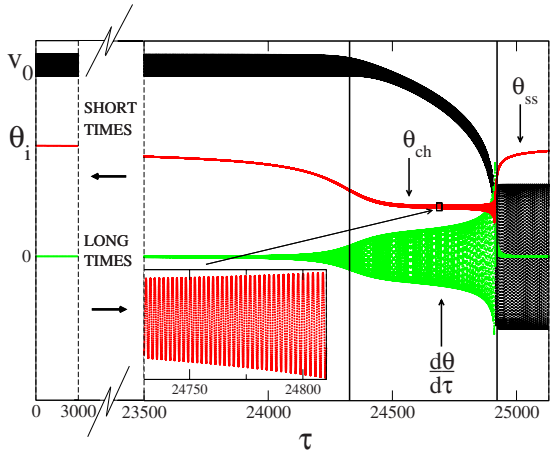

FIG. 2. (Color online) Evolution with respect to the dimensionless time τ of the center of mass velocity $v(\tau)$, the orientation angle $\theta(\tau)$, and the angular velocity $d\theta(\tau)/d\tau$ for $\gamma=4$ and the initial condition that the dimer is thrown with dimensionless initial velocity $v_0=8\pi$ and $\theta_i=1.54$. Three time regimes are seen. In the first, the center of mass velocity oscillates rapidly around a value higher than the initial value, the orientation remains close to its initial value, and the angular velocity is essentially zero. In the graph, this first regime is so long that we have shown it split into a short time part and a long time part. In the second regime, the center of mass velocity decreases in power law fashion, the orientation switches to a different constant around which it oscillates with small amplitude, and the angular velocity increases its oscillations significantly. The inset shows that the angle oscillates even where it appears to be a constant. In the third regime, the center of mass velocity changes its evolution from the power law to oscillations but now around the value zero, the amplitude of the oscillations decreasing apparently not at all or very slowly (not appreciable in the graph). In this third regime, the orientation switches to another constant value and the angular velocity vanishes. The transition between the second and third regimes is quite abrupt.

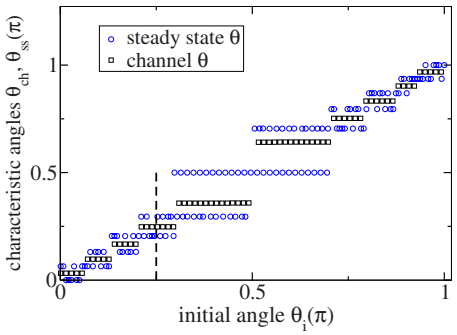

FIG. 3. (Color online) Curious patterns displayed by characteristic dimer orientations θ_{ch} and θ_{ss} in the second and third regimes respectively, and their dependence on the initial angle the dimer makes to the vertical. The plot is constructed as the result of over a thousand numerical runs for various initial angles, all carried out for $\gamma=4$, $\zeta=5\pi$, and $v_0=8\pi$, but only a subset has been displayed to make the visual appreciation clearer. Each run has resulted in one value of θ_{ch}, the channel angle the dimer stays around in the second regime (denoted by a square) and one value of θ_{ss}, the steady state angle the dimer goes to, in the third regime. Our findings show that, for a given value of ζ, two values of θ_{ss} correspond to every value of θ_i, whereas θ_{ch} is determined uniquely by the initial inclination to the vertical. Changing the value of ζ changes the entire family of each type of orientation.

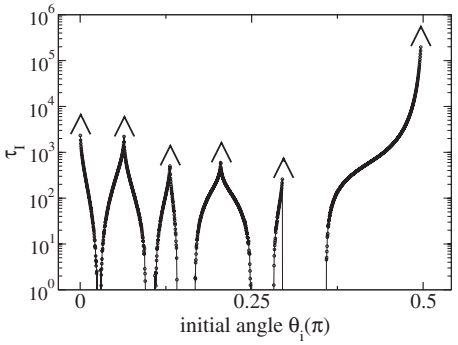

FIG. 4. Semilogarithmic plot of the time before dissipation begins, i.e., the time span τ_I of the first regime of time evolution before the center of mass velocity begins to decay, as a function of the initial orientation of the dimer, for a given value of ζ. The time generally increases until the initial orientation becomes horizontal $(\theta_i=\pi/2)$ when it becomes infinite. The time also grows without bound at several intermediate values of θ_i. We have indicated these surges to infinity in the plot by placing circumflex symbols on top of the curve. The corresponding θ_i values are precisely θ_{ss}. Parameter values used in the present plot are $\gamma=4$ and $\zeta=5\pi$.

units and the other starting at $\tau=2.35\times10^4$. In the second regime of the evolution, the center of mass velocity is seen to exhibit quite different behavior in that $v(\tau)$ decreases, signifying damping. The decrease of the velocity proceeds in power law fashion. The third regime starts when the center of mass velocity reaches zero. Now $v(\tau)$ oscillates with large amplitude and very little apparent damping.

Corresponding to these three regimes in translational motion, the rotational motion also shows three types of behavior. In the first regime, the orientation remains close to its initial value, the angular velocity being largely zero. In the second regime, the orientation switches to a different constant around which it oscillates with small amplitude, and the angular velocity keeps increasing its oscillations significantly. In the third regime, the angular velocity vanishes and the orientation takes on yet another constant value.

Features of these numerical observations that are noteworthy include sharp changes in the time evolution in three regimes, the abruptness of the second transition, and the fact that the two constant values of the inclination to the vertical attained in the second and third regimes appear to form entire families of angle values with curious properties. Which member of each family is selected by the system to evolve into appears to depend on the initial inclination. The families themselves are, however, independent of the initial conditions. To clarify this numerical observation, we show Fig. 3, which has been constructed by performing over a thousand numerical runs, each run resulting in one circle and one square.

We assign the term "channel angle" to the inclination around which the dimer stays in the second regime and denote it by θ_{ch}. Similarly we use the term 'steady state angle' for the value the inclination goes to eventually, i.e., in the third (final) regime, and denote it by θ_{ss}. In Fig. 3, we plot the dependence of θ_{ch} (squares) and θ_{ss} (circles) on the initial angle θ_i. We see that θ_{ch} exhibits discrete values, 10 such values being apparent in the plot: 0.1, 0.3, 0.53, 0.78, 1.13, 2.0, 2.4 2.6, 2.8, and 3.0. Similarly we can see in the plot 11 values of θ_{ss}: 0.0, 0.20, 0.41, 0.64, 0.92, $\pi/2$, 2.2, 2.5, 2.72, 2.94, and π. All of these 11, except for the central value $\pi/2$, have been determined via numerical runs. Simulation time increases enormously as θ_i approaches $\pi/2$ but it is very clear from the numerical work that, as we carry out the runs for longer and longer times, the central value of θ_{ss} in all cases approaches $\pi/2$. We have shown that limiting value in the plot. The totality of numerically found values, displayed in Fig. 3, form a curious pattern in that they are interlaced (they alternate) and each corresponds to definite finite spans of θ_i. The spans overlap in the case of neighboring θ_{ss} but not in the case of neighboring θ_{ch}. For every value of θ_i, the initial inclination to the vertical, two values of θ_{ss} but only one value of θ_{ch} are possible. Which θ_{ss} is picked by the system depends on the initial value of the velocity of the center of mass. For instance, as shown by the dotted vertical line drawn at the arbitrarily chosen value $\theta_i=0.8$, θ_{ch} can have only the value 0.78 whereas θ_{ss} may become either 0.64 or 0.92.

Initial orientation has a profound effect on the time span of the first regime, i.e., the time before dissipation begins to occur in the center of mass motion. We show this in Fig. 4 where we have plotted τ_I, the time before dissipation, defined as the time until $v(\tau)$ begins to drop, as a function of the initial orientation for the parameter values. We see that τ_I generally increases until the initial orientation becomes horizontal $(\theta=\pi/2)$ and then becomes infinite. It also becomes infinite at smaller values of θ_i. Careful inspection reveals that this happens at $\theta_i=\theta_{ss}$. Parameter values are as shown in the plot.

The time span of the second regime, τ_{II}, which begins when $v(\tau)$ begins to decay and ends when it reaches 0, also

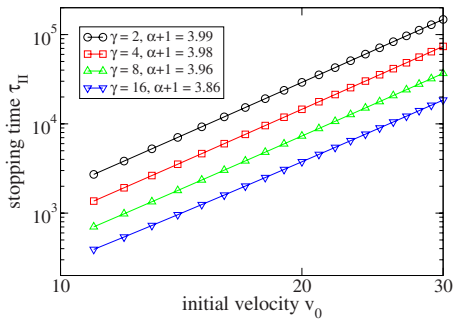

FIG. 5. (Color online) Double logarithmic plot of τ_{II}, the time span of the second regime of time evolution in which the center of mass velocity drops from its initial oscillations above v_0 to 0, for four different values of the damping coefficient as shown. We have determined the time span by carrying out runs for $\theta_i = \theta_{ch}$ which results in the disappearance of the first regime. The straight lines signify that $v(\tau)$ obeys a power law. The slope $\alpha+1$, which the plot shows to be 4 within experimental error, means that the evolution proceeds such that $dv/d\tau$ is proportional to $-1/v^{\alpha}$, with $\alpha \approx 3$. Parameter values are $\gamma=4$, $\theta_i=0.7$, $\zeta=\pi$.

shows interesting dependence on the system parameters. In Fig. 5 we display, through a double logarithmic plot, the remarkably linear relationship between the logarithms of τ_{II} and of the initial velocity of the center of mass. The linear relationship is seen for several values of the damping coefficient γ and means, obviously, that the dependence of τ_{II} on $v(\tau)$ is of the power law form. The exponent of the power law is unmistakably 4 within numerical error.

We thus see that the initial orientation of the dimer determines key elements of the time evolution of the system. Let us consider Figs. 2–5 as our primary numerical results. Time evolution with its three regimes separated by transitions, with power law decay of the center of mass velocity in the second regime, is the first result. Patterns of characteristic angles in the second and the third regimes, θ_{ch} and θ_{ss}, and their special dependence on the initial angle θ_i (as well as on ζ) constitute the second result. Highly structured dependence of the time span of the first regime on the initial orientation forms the third result. And the linear dependence, in a double logarithmic plot, of the time span of the second regime on the initial center of mass velocity is the fourth result.

III. ANALYTIC UNDERSTANDING

Of the large number of intriguing numerical observations that we have collected above, we select a few and begin our analysis with the following questions:

(1) What is the significance of the specific values we find for the characteristic angles, θ_{ss} and θ_{ch}, and of their interlacing patterns including the overlapping spans of θ_i to which they correspond?

(2) What is the detailed nature of the oscillations displayed by the center of mass velocity in the first and third regimes?

(3) Why is a power law present in the decay of the velocity in the second regime and why is the power exponent 3?

We address these three questions in Secs. III A–III C, respectively. We then carry out a comparison of our simple theory to the simulations in 3.4 and explore the relationship of our rotational model to a vibrational model in 3.5.

A. Characteristic orientations θ_{ss} and θ_{ch}: Understanding Figs. 3 and 4

Our attempts at an analytic understanding of the various observations described above begin with the second of Eqs. (2). The presence of the dissipative term $-\gamma\dot{\theta}$ ensures that at long times θ will tend to a constant and both time derivatives of the angle will vanish. In that steady state, the angle θ will be either a multiple of $\pi/2$ or a root of the equation

$$\sin(\zeta \sin \theta) = 0. \tag{3}$$

The value of $\pi/2$ corresponds to initially placing the dimer parallel to the horizontal. The substrate forces which are always horizontal can produce no torque on the dimer which, therefore, does not turn at all during evolution. For any other initial angle, there is a torque at first but it vanishes when the eventual orientation attained by the dimer is a root of Eq. (3). All these roots of Eq. (3) indeed turn out to be precisely the steady state values we have observed in the third regime and called θ_{ss}. In the case of the characteristic orientations θ_{ch} of the second regime, we have found out, empirically, that they are all very nearly roots of $\cos(\zeta \sin \theta)=0$. For this condition, the first of Eqs. (2) shows that the acceleration of the center of mass vanishes. We can thus conclude that in the second regime, the constants to which the dimer orientation tends, correspond to nearly vanishing center of mass acceleration.

There is a curious geometrical interpretation we can assign to both the characteristic angles. When the dimer orientation to the vertical is θ_{ss}, the projections on the horizontal line of the locations of the two masses are precisely in the same phase of the substrate potential. The horizontal forces then produce no torque on the dimer and do not contribute to its rotation. When the dimer orientation is, on the other hand, θ_{ch}, the projections of the two masses occupy opposite phases of the substrate potential. The horizontal forces then produce the maximum torque possible and contribute strongly to the rotation. This is completely compatible with the observation from Fig. 2 that the angular velocity is nonvanishing only in the second regime in which the dimer stays around θ_{ch}. Of the two dimer orientations that we have depicted in Fig. 1 to illustrate the model pictorially, the lower orientation (smaller angle) corresponds to one possible value of θ_{ss} and the upper orientation (larger angle) to an angle close to one possible value of θ_{ch}. In the former case, the substrate forces are equal in magnitude and direction, and produce no turning effect on the dimer. In the latter case they are equal in magnitude but opposite in direction, and so do produce a turning effect. The torque is maximum at the phase relative to the substrate potential shown in the plot. Needless to say, both families of orientations depend crucially on ζ, i.e., on the magnitude of the length of the dimer relative to the substrate potential wavelength.

The content of Figs. 3 and 4, gathered directly from the simulations, can be thus explained simply from the fact that the characteristic orientations are the roots of Eq. (3) which yield θ_{ss} and of

$$\cos(\zeta \sin\theta) = 0, \tag{4}$$

which yield θ_{ch}. The former condition corresponds to the eventual inclination into which the dimer settles whereas the latter marks maximization of the torque on the dimer and minimization of the center of mass acceleration. We also see that the first regime of the center of mass velocity evolution, where the velocity shows no damping, would last forever if $\theta_i = \theta_{ss}$. This is clearly the reason for the surges to infinity observed in Fig. 4.

B. Oscillations of $v(\tau)$ in the first and third regimes: Understanding Fig. 2

Taking advantage of the numerically found observation that the angle θ remains largely constant in each of the three regimes, first around the initial value θ_i, then around the channel value θ_{ch}, and finally around the steady state value θ_{ss}, let us ask for the solution of the first of Eqs. (2) if θ is constant. Let us represent the magnitude of $\cos(\zeta \sin\theta)$ by the symbol A,

$$A = |\cos(\zeta \sin\theta)|. \tag{5}$$

Let us also recall [8] that the equation

$$\frac{d^2Y}{dz^2} + \sin Y(z) = 0 \tag{6}$$

encountered in the analysis of the physical pendulum can be solved in terms of Jacobian elliptic functions dn or cn. Thus, for instance, if the value of dY/dz at $z=0$ is denoted by $\mathcal{V}_0$, Eq. (6) is known to have the solution

$$\frac{dY(z)}{dz} = \mathcal{V}_0 \mathrm{dn}\left(\frac{\mathcal{V}_0 z}{2}, \frac{2}{\mathcal{V}_0}\right), \tag{7}$$

where $2/\mathcal{V}_0$ is the elliptic modulus and $\mathcal{V}_0 z/2$ is the argument of the dn. We use this result and the scaling $z = \sqrt{A}\tau$ in the first of the Eqs. (2) to obtain the following solution for an initial velocity v_0,

$$v(\tau) = v_0 \mathrm{dn}\left(\frac{v_0\tau}{2}, \frac{2\sqrt{A}}{v_0}\right). \tag{8}$$

This form of the solution is particularly convenient if v_0 is large enough to satisfy $v_0 > 2\sqrt{|\cos(\zeta \sin\theta)|}$.

It is well known that the dn function has precisely the qualitative behavior shown by the center of mass velocity in Fig. 2 in the first regime, with its oscillations around a nonzero average value. Indeed, it will be shown graphically below (in Fig. 6) how close the coincidence of the numerically found $v(\tau)$ in the first regime in Fig. 2 is with the simple dn prediction of our analytic treatment here.

By the time the third regime is reached, the velocity will have dropped to low enough values that application of the same approximate physical pendulum solution as in Eq. (8) is best done by performing the Jacobi transformation. This transformation proceeds in the standard manner [8] by changing the dn function to cn, simultaneously flipping the elliptic modulus and multiplying the argument and original elliptic modulus to produce the new argument. Thus, in the third regime, our approximate analytic description from Eqs. (2) is

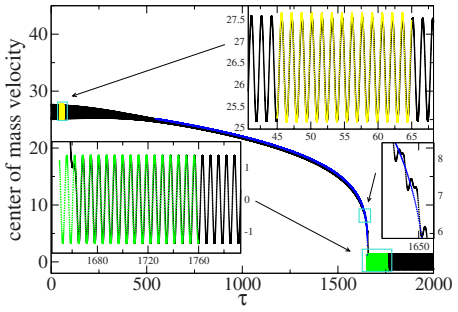

FIG. 6. (Color online) Comparison of simple analytic theory with numerical simulations carried out separately in the three regimes. The parameters used to make this figure in the simulations are $\zeta = 5/\pi$, $\theta_i = 1.3$, $v_0 = 8\pi$, $\gamma = 4$. The three insets are the result of zooming on the three regimes and show remarkable agreement between simulations and the proposed analytical expressions in terms of the Jacobian elliptic functions and the power law. The top right inset shows the simple dn solution of Eq. (8) for the first regime as the light line and the numerical solution as the dark line. The bottom left inset displays for similarly for the third regime our cn solution (9) compared to the simulation. The coincidence in both insets is remarkable. The middle right inset reproduces the average power law decay given by our Eq. (15) with impressive precision.

$$v(\tau) = v_0^1 \mathrm{cn}\left(\sqrt{A}\tau, \frac{v_0^1}{2\sqrt{A}}\right) = v_0^1 \mathrm{cn}\left(\tau, \frac{v_0^1}{2}\right), \tag{9}$$

in which the extreme right hand side has been written using the fact that in the third regime the orientation attains the steady state value θ_{ss} quickly, after which A has the limiting value 1. The initial velocity value v_0^1 in this (third) regime is not the same as v_0 but is the maximum value the velocity takes on after the damping that it undergoes in the second regime.

The cn function oscillates around the value zero in complete qualitative agreement with what is observed numerically for the center of mass velocity in the third regime in Fig. 2. It will be seen below (in Fig. 6) that the quantitative agreement is excellent also in this regime.

C. Power law decay of $v(\tau)$ in the second regime: Understanding Figs. 2 and 5

To understand the power law decay of $v(\tau)$ in the second regime, we first turn to the second Eq. (2), use the knowledge that the rotational angle remains in the second regime close to θ_{ch} which means that $\sin(\zeta \sin\theta) \approx 1$, and rewrite the equation as

$$\ddot{\theta} + \gamma\dot{\theta} = [(1/\zeta)\cos\theta_{ch}]\cos y. \tag{10}$$

Keeping in mind that the rotational angle undergoes much faster oscillations in this regime than the center of mass velocity, we may regard this equation as describing the absorption of energy by a damped free particle driven by a (co)sinusoidal force of frequency proportional to the center of mass velocity. The displacement of the hypothetical free par-

ticle is θ, the damping rate is γ and the strength of the driving agency is $(1/\zeta)\cos\theta_{ch}$.

We now borrow an energy balance argument presented in the context of a related model in the literature consisting of a dimer like ours moving under the action of a sinusoidal substrate potential and executing internal motion which is *vibrational* rather than rotational [9–13]. The essence of the argument as applied to our case here is based on the fact that, as the result of the coupling provided by the masses feeling different substrate forces, the internal (rotational) coordinate absorbs energy from the center of mass motion. The energy *lost* by the center of mass can be obtained by calculating the energy *gained* by the rotational coordinate. A standard textbook absorption calculation yields the cyclic average of the latter. The time rate of the center of mass velocity can be calculated from the time rate of the center of mass kinetic energy.

Resolving $\cos y = \cos[\int_0^\tau v(s)ds]$ into its Fourier components with frequencies ω_i and calling the product of $(1/\zeta)\cos\theta_{ch}$ with each corresponding Fourier coefficient as B_i, we can rewrite Eq. (10) as

$$\ddot{\theta} + \gamma\dot{\theta} = \sum_i B_i \cos\omega_i\tau. \tag{11}$$

The angle θ may be decomposed into components θ_i each of which satisfies, after transients have died down,

$$\theta_i(\tau) = \frac{B_i}{\sqrt{\omega_i^4 + \omega_i^2\gamma^2}}\cos(\omega_i\tau - \delta_i). \tag{12}$$

Here the lag factor δ_i equals $\tan\delta_i = \gamma/\omega_i$. Absorption of energy from the center of mass motion into the rotational coordinate occurs at a rate which equals the product of the torque and the angular velocity, and is proportional to

$$\gamma\left(\frac{\cos\theta_{ch}}{\zeta}\right)^2 \sum_i \frac{B_i}{\omega_i^2 + \gamma^2}.$$

Let us now (i) restrict the analysis as in Ref. [11] to situations in which we can replace the i sum by a single term involving an average frequency ω_a, so that we have

$$\cos\int_0^\tau v(s)ds \approx \cos\omega_a\tau, \tag{13}$$

ω_a being equal, in the system of units used, to the center of mass velocity v, (ii) calculate the rate of dissipation of the center of mass kinetic energy which is proportional to $d/d\tau(1/2)(2mv^2)$, and (iii) equate the two rates to get the general power law of decay of velocity,

$$\frac{dv}{d\tau} = -\frac{\gamma}{2}\frac{\cos^2\theta_{ch}}{v(v^2+\gamma^2)}. \tag{14}$$

If v is much larger then the damping rate γ, which is the case in our simulations (in the second regime where this decay of velocity is occurring), we have

$$\frac{dv}{d\tau} = -\frac{\gamma}{2}\frac{\cos^2\theta_{ch}}{v^3}. \tag{15}$$

For further details we refer the reader to the earlier literature [11] on the vibrational dimer. The difference in our case relative to that in Ref. [11] is that the absorbing entity is, as Eq. (10) shows, a free particle rather than a harmonic oscillator. Equation (15) yields power law behavior with the correct exponent. The exponent in the velocity decay equation is 3. The solution therefore gives, for τ_{II}, the extent of the second regime (of Fig. 2), as shown in Fig. 5, a power law dependence on initial velocity with exponent 4,

$$\tau_{II} = \frac{v_0^4}{2\gamma\cos^2\theta_{ch}}. \tag{16}$$

D. Comparison of approximate analytics with numerical $v(\tau)$: Understanding Figs. 2 and 6

Equations (8), (9), and (15) provide our (approximate but simple) analytical description of the evolution of the center of mass velocity in the three regimes shown in Fig. 2. Jacobian elliptic functions provide the description in the first and the third regimes and the power law form in the second regime. We display Fig. 6 to show a comparison of our analytic predictions for the explicit time dependence of $v(\tau)$ to the numerical findings. The comparison is displayed separately for each of the three regimes.

We see a remarkable coincidence in each of the three regimes. Except for taking the initial v_0^1 from the simulations and adjusting the phase of the analytic expression for a fit at a single point of time, no modifications of any kind have been made to the analytic results as derived. Also, the two adjustments have been made only in the third regime. The agreement of the amplitude of the cn solution is essentially perfect. Also, the analytical prediction and the simulation remain in phase for a prolonged time. The agreement is also excellent in the first regime. In this regime the theoretical curve shows slightly larger amplitude in the case of the dn solution. This arises from the fact that the very weak decay of the amplitude is not represented by the solution. The second regime fit is also noteworthy. The power law is followed faithfully on the average as the plot shows.

E. Relationship of the rotational to the vibrational system

It is instructive to compare the rotational dimer we have investigated in the present paper to the vibrational dimer analyzed earlier in the literature [11–13] and enquire into the precise relationship that they bear to each other. In both systems, the masses comprising the dimer experience the substrate forces in essentially the same manner. Because the substrate forces act only in the horizontal direction, we consider the locations of the two masses in the vibrational system but only *the projections of the locations* along the horizontal in the rotational system. Although the rotational dimer is rigid, the projection along the horizontal of the location of one of the masses relative to the other varies in time. The variation is that of a harmonic oscillator with a finite spring constant in the vibrational dimer. The corresponding spring constant is zero in the rotational dimer. This is a very important difference. It is responsible for the fact that the energy

balance argument used in Sec. III C to derive the power law of the decay of the center of mass velocity looks upon the internal coordinate as representing a free particle (zero natural frequency) rather than a bound particle (finite natural frequency) which was true in the case of the vibrational dimer [11].

Because the natural frequency is zero for the rotational dimer, one might be tempted to consider the latter to be less complex than the vibrational dimer. However, it is actually considerably more complex when viewed from another point of view: the actual motion (rotation) of the dimer is planar rather than linear which is the case in the vibrational dimer. The Lagrangian of the vibrational dimer [11,13] is

$$m\left[\left(\frac{dx}{dt}\right)^2+\left(\frac{dx_-}{dt}\right)^2\right]-k(x_-^2-ax_-)$$
$$-2u_0\cos\left(\frac{2\pi x}{b}\right)\cos\left(\frac{2\pi x_-}{b}\right),$$

where k is the spring constant of the vibration, $x=(1/2)(x_1+x_2)$ is the center of mass coordinate and $x_-=(1/2)(x_1-x_2)$ is the internal coordinate. The locations of the two masses are denoted by x_1 and x_2. Making the same scale transformations as made for the rotational case at the beginning of the present paper, introducing a damping term, and additionally writing the internal coordinate as

$$\xi=\frac{x_1-x_2-a}{a}=\frac{2\pi x_-}{b\zeta}-1, \tag{17}$$

we obtain the vibrational counterpart of the starting Eqs. (2) for the rotational dimer analyzed in the present paper,

$$\ddot{y}=(\sin y)\cos[\zeta(1+\xi)],$$

$$\ddot{\xi}+\Omega^2\xi=(1/\zeta)(\cos y)\sin[\zeta(1+\xi)]-\gamma\dot{\xi}. \tag{18}$$

The natural frequency of the vibration, in the dimensionless units used, is

$$\Omega=\left(\frac{2\pi}{b}\right)\sqrt{\frac{2k}{u_0}}. \tag{19}$$

Equations (18) are identical to those in Ref. [11], but written here in our dimensionless units.

Comparison of the rotational Eqs. (2) to the vibrational Eqs. (18) reveals the presence of the natural frequency term in the latter which does not appear in the former case since rotation has no stiffness. The comparison also shows that the rotational dynamics has the more complex trigonometric factors appropriate to rotation. The terms describing the coupling of the center of mass motion to the internal motion are similar to each other except that the linear factor $1+\xi$ appears in the vibrational case but the nonlinear $\sin\theta$ in the rotational case.

The evolution of the rotational system for *small angles* to the vertical is similar to that of the vibrational system. However some distinct differences exist. To appreciate the similarities and differences, notice that the vibrational Eqs. (18) can be rewritten without approximation in the form

$$\ddot{y}=(\sin y)\cos\zeta z,$$

$$\ddot{z}+\Omega^2(z-1)=(1/\zeta)(\cos y)\sin\zeta z-\gamma\dot{z}, \tag{20}$$

simply by introducing a different internal coordinate $z=1+\xi$. This equation can be also obtained from the rotational Eqs. (2) for small angles θ *by approximating* $\sin\theta\approx\theta$ and calling this approximated small angle as z. Although the form of the equations is identical in the two cases, the physical requirement that $z\approx 0$ in one case (rotational for small angles) is incompatible with $z\approx 1$ in the other (vibrational.) A basic difference thus persists in addition to the presence of the stiffness in the vibrational case.

On the other hand, the similarities permit the analytic arguments given for the rotational system in the present paper to provide a much deeper understanding of our earlier studies [11–13] of the vibrational system. The vibrational work had focused only on what we have called the second regime in the present paper, in particular the power law observed in the evolution of the center of mass velocity. The present discussion, along with simulations we have now carried out after the rotational analysis, also shows that the other two regimes exist in the vibrational system as well.

Inspection of Eq. (20) shows that the damping term is proportional to $-\gamma\dot{z}$ that is to $-\gamma(\cos\theta)\dot{\theta}$. The effective damping is thus controlled in the rotational system by $\gamma\cos\theta$ and becomes therefore very small for initial orientations that are nearly horizontal, i.e., for *large* rather than small angles. This is so because $\cos\theta\approx 0$ as $\theta\approx\pi/2$. It is this smallness of the effective damping for large initial angles that led us to the observation of the first regime in the rotational system. The regime was practically invisible in earlier studies of the vibrational system.

There appears to be one fundamental difference between the rotational and the vibrational systems, however. In the third regime, as the orientation settles into one of the values of θ_{ss}, the projections of the dimer end locations along the horizontal acquire equal phases of the substrate potential. Absence of any spring forces means then that the coupling of the rotational to the center of mass motion completely vanishes. The center of mass (as well as each mass) oscillates along the horizontal forever and the amplitude of the oscillations does not decay. This is a peculiar result which does not hold in the vibrational system. At the corresponding stage of the time evolution, except for special values of ζ, equivalently of the dimer length to substrate wavelength ratio, the two masses in the vibrational system experience forces in opposite directions. The coupling persists and the energy of the entire system, including that resident in the center of mass velocity oscillations, decays slowly.

IV. CONCLUDING REMARKS

In summary, we have analyzed a simple model of interest to the subject of molecules experiencing friction while moving on material surfaces and performing internal motion. Despite its simplicity, the model has displayed a richness of phenomena. We have described only some of them here. Clearly, all the phenomena we have found and discussed so

far are responses of the system to an initial translational velocity until the movement of the center of mass ceases. In other words it is about the transient regime. While that could be limited to short periods of time, we have to consider that in many practical situations what is important is precisely that regime; i.e., when a system is perturbed from its steady state and we want to understand how the energy dissipates until it gets to its new equilibrium. There is a whole additional dimension of effects we have discovered when steady forces are applied and when the dimer is initially thrown with a high angular velocity. The steady force simulations display hysteresis and related effects. The high initial angular velocity allows the rotational motion to sample all angles and appear to involve dynamic localization effects [14,15] not accessible in the regimes we have analyzed here. Generalizations of the friction law in the related vibrational dimer, described by Tiwari *et al.* [13], also have their counterparts in the rotational dimer as we have found. [For an example of the generalizations, see Eq. (14) in the present paper.] We intend to address these numerous observations in a forthcoming publication.

The underlying equations of motion for the analysis in the present paper are Eqs. (2). The primary findings are in Figs. 2–5. We have provided an explanation of some of the observed features on the basis of very simple analytic arguments. The explained features include the meaning of the patterns displayed by the characteristic orientations θ_{ss} and θ_{ch} and their dependence on the ratio of the dimer length to the substrate wavelength, the source of the power law, the surges to infinity at some values of the initial orientation, and the essential source of the time evolution of the center of mass velocity. Figure 6 compares our simple analytic predictions for the time dependence of the center of mass velocity with the observed simulations. Our three analytic expressions, two in terms of elliptic functions and the third in terms of the derived power law, are in remarkable coincidence with the simulations. The coincidence should leave no doubt that the essence of the phenomenon has been captured by the simple analytics we have provided.

Among the features that we have not been able to explain as yet, to our satisfaction, are the source of the constancy of the dimer orientations. Indeed our analytical work described above takes this constancy (observed in the simulations) as an input and delivers as an output an understanding of the time dependence of the center of mass velocity (not only qualitatively but quantitatively as well.) It is also possible to do the reverse, i.e., taking the observed center of mass motion as an input we can understand to some extent the rotational features. For instance, notice that the center of mass velocity performs rapid oscillations around a constant value which means that the cosine of the center of mass displacement forces the first term on the right hand side in the second of Eqs. (2) to oscillate very fast from positive to negative values. The average is vanishing and since the second term on the right hand side is small (because we start the dimer with zero angular velocity), the orientation of the dimer remains largely unchanged. This can be considered a partial explanation of what is observed for the orientational motion in Fig. 2. It is also interesting to notice that the orientational dynamics display features of parametric oscillation, the evolution of the center of mass providing the temporal variation of an effective rotational frequency in Eqs. (2). It is our conjecture that the imperceptibly slow decay of the center of mass velocity, not discernible in the first regime, eventually brings the velocity (equivalently the parametric oscillator frequency) within the so-called parametric window [16] and that this marks the perceptible power law decay of the velocity, i.e., the beginning of the second regime. We hope that these open questions that remain unanswered will be explained by readers of our paper through deeper insights than we have been able to gain.

Despite the apparent simplicity of the laws of macroscopic friction's laws, the underlying dynamics of sliding surfaces (macroscopic or not), and the diffusion of molecules or cluster over surfaces [7] are complex nonequilibrium, nonlinear phenomena resulting from intricate interplay of multiple processes [17]. We are well aware that the dynamics of a single rotating dimer constrained to slide in a one-dimensional potential is far from able to account for the many effects that underlie the microscopic origin of friction. However the richness that emerges from our simplified model is a sample of how complex and subtle the long standing problem of the elucidation of friction features can be. By itself, the simple model considered is able to show a rich repertoire of intricate dynamical manifestation of microscopic sliding friction of a single dimer: going from almost frictionless sliding to static friction, through a resonant strong dissipation, all emerging from the coupling between rotation and translation. It provides an essential ingredient in the assembling of an atomistic and realistic model of friction.

ACKNOWLEDGMENTS

This work was supported in part by the National Science Foundation under Grant No. INT-0336343. I. G. Neide and S. Gonçalves acknowledge support from Conselho Nacional de Desenvolvimento Científico e Tecnológico (CNPq, Brazil).

[1] F. P. Bowden and D. Tabor, *The Friction and Lubrication of Solids*, 2nd ed. (Clarendon, Oxford, 1986).
[2] G. Amontons, *De La Resistance Causée dans les Machines* (Mémoires de l'Académie Royale des Sciences, Paris, 1699).
[3] C. A. Coulomb, *Théorie des Machines Simples* (Mémoires de Mathématique et de Physique de l'Académie Royale des Sciences, Paris, 1785).
[4] J. Krim, Surf. Sci. **500**, 741 (2002).
[5] B. N. J. Persson, *Sliding friction: Physical Principles and Applications* (Springer-Verlag, Berlin, 1998).
[6] B. Bhushan, J. N. Israelachvili, and U. Landman, Nature (London) **374**, 607 (1995).

[7] M. Evstigneev, S. von Gehlen, and P. Reimann, Phys. Rev. E **79**, 011116 (2009).
[8] See, e.g., F. Bowman, *Introduction to Elliptic Functions with Applications* (Dover Publications, New York, 1961).
[9] T. Strunz and F.-J. Elmer, Phys. Rev. E **58**, 1601 (1998).
[10] C. Fusco and A. Fasolino, Thin Solid Films **428**, 34 (2003); see also C. Fusco, A. Fasolino and T. Janssen, Eur. Phys. J. B **31**, 95 (2003).
[11] S. Gonçalves, V. M. Kenkre, and A. R. Bishop, Phys. Rev. B **70**, 195415 (2004).
[12] S. Gonçalves, C. Fusco, A. R. Bishop, and V. M. Kenkre, Phys. Rev. B **72**, 195418 (2005).
[13] M. Tiwari, S. Gonçalves, and V. M. Kenkre, Eur. Phys. J. B **62**, 459 (2008).
[14] D. H. Dunlap and V. M. Kenkre, Phys. Rev. B **34**, 3625 (1986); **37**, 6622 (1988); D. H. Dunlap, V. Kovanis, R. V. Duncan, and J. Simmons, *ibid.* **48**, 7975 (1993).
[15] V. M. Kenkre and S. Raghavan, J. Opt. B: Quantum Semiclassical Opt. **2**, 686 (2000); V. M. Kenkre, J. Phys. Chem. B **104**, 3960 (2000).
[16] L. D. Landau and E. M. Lifshitz, *Mechanics*, 3rd ed. (Butterworth-Heinemannn, Oxford, 1976).
[17] M. Urbakh and E. Meyer, Nature Mater. **9**, 8 (2010); S. M. Rubinstein, G. Cohen, and J. Fineberg, Nature (London) **430**, 1005 (2004).